Localization of wave patterns on classical periodic orbits in a square billiard

Y. F. Chen* and K. F. Huang
Department of Electrophysics, National Chiao Tung University, 1001 TA Hsueh Road, Hsinchu, 30050, Taiwan

Y. P. Lan
Institute of Electro-Optical Engineering, National Chiao Tung University, Hsinchu, Taiwan

(Received 20 June 2002; published 22 October 2002)

The connection between wave functions and classical periodic trajectories in a square billiard is analytically constructed by using the representation of SU(2) coherent states. The analytical function form is modified to show that the wave patterns can be apparently localized on the classical periodic trajectories by superposing a few nearly degenerate eigenfunctions. Based on the analogy between the Schrödinger and Helmholtz equations, the features of wave functions are experimentally studied from the transverse pattern formation in a laterally confined microcavity laser. The experimental transverse pattern in a square-shaped microcavity agrees very well with the constructed wave pattern concentrated along classical periodic orbits.

DOI: 10.1103/PhysRevE.66.046215 PACS number(s): 05.45.Mt; 03.65.−w; 42.60.Jf

I. INTRODUCTION

The two-dimensional (2D) square billiard is one of the simplest billiards that is completely integrable in classical mechanics [1,2]. One common periodic orbit in a 2D square billiard is usually denoted by (1,1). As shown in Fig. 1, the (1,1) periodic orbits can be characterized by a parameter ϕ that is related to the wall positions of specular reflection points [3,4]. Some examples of periodic orbits are shown in Fig. 1. According to Bohr's correspondence principle, the classical limit of a quantum system should be achieved when the quantum numbers go to infinity. However, the conventional eigenstates of a square billiard in most quantum mechanics do not manifest the properties of classical periodic orbits even in the correspondence limit of large quantum numbers.

Although semiclassical periodic orbit theory has been used to explain the scarred wave functions in quantum chaos [5–7], the wave functions related to stable periodic orbits seem to have been overlooked. The reason for this disregard is probably that most work has focused on energy levels and energy level statistics [8–10]. Furthermore, there are some striking phenomena in open quantum ballistic cavities associated with the wave functions in terms of classical periodic orbits [11–13]. Therefore, to construct the connection between the eigenfunctions and classical periodic trajectories is essentially helpful for understanding quantum-classical correspondence as well as quantum transport in mesoscopic systems.

In this paper, we use the representation of SU(2) coherent states [14,15] to analytically construct the wave functions related to the classical periodic trajectories in the 2D square billiard. The noticeable finding is that a superposition containing only a few nearly degenerate eigenfunctions is already sufficient for localization of the wave function intensity on the classical periodic trajectory. This result explains the reason why the wave functions related to classical periodic orbits often appear in weakly perturbed integrable systems [16,17]. In experiment, the analogy between the Schrödinger and Helmholtz equations [18] enables us to connect the features of wave functions with the transverse modes in a laterally confined microcavity laser. The experimental transverse pattern in a square-shaped cavity is generally found to be concentrated along classical periodic orbits. This result confirms that the wave functions related to classical periodic orbits provide a more physical description of a phenomenon than the true eigenstates in mesoscopic systems.

II. WAVE FUNCTIONS RELATED TO CLASSICAL PERIODIC ORBITS

Recently, Pollet *et al.* [19] demonstrated that the wave function of the SU(2) coherent state for 2D quantum harmonic oscillation is particular simple and well localized on the corresponding classical elliptical trajectory. Mathematically, the SU(2) coherent state for 2D quantum harmonic oscillation is a superposition of eigenstates leading to a state with a minimum uncertainty of $\Delta x \Delta y$, where x and y are the Cartesian coordinates [14,15]. For 2D integrable Cartesian systems, the SU(2) minimum-uncertainty states $\Psi_N(x,y;\tau)$ can be expressed as the superposition of number eigenstates $\psi_{K,N-K}(x,y)$ where N is an integer constant and $K=0,1,2,...,N$:

$$\Psi_N(x,y;\tau)=(1+|\tau|^2)^{-N/2}\sum_{K=0}^{N}\binom{N}{K}^{1/2}\tau^K\psi_{K,N-K}(x,y). \tag{1}$$

The parameter τ is, in general, complex and has a physical meaning in that $|\tau|^2$ is the ratio of the average values of two quantum numbers. In the limit $\tau\to 0$ (or $\tau\to\infty$), the SU(2) coherent states becomes the eigenstate $\psi_{0,N}(x,y)$ [or

*Author to whom correspondence should be addressed. FAX: (886-35) 729134. Electronic address: yfchen@cc.nctu.edu.tw

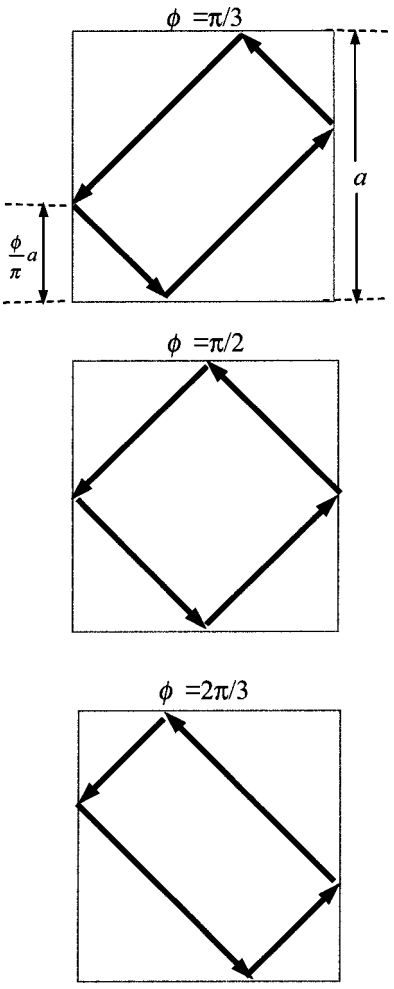

FIG. 1. Some classical periodic orbits. The periodic orbits are in terms of the parameter ϕ which is related to the wall positions of specular reflection points.

$\psi_{N,0}(x,y)]$. In terms of the eigenstates of a 2D square billiard, $\psi_{K,N-K}(x,y)$ is given by

$$\psi_{K,N-K}(x,y)=\frac{2}{a}\sin\left[(K+1)\frac{\pi x}{a}\right]\times\sin\left[(N-K+1)\frac{\pi y}{a}\right],\quad K=0,1,...,N, \tag{2}$$

where a is the length of the square boundary. The numerical calculation reveals that the classical periodic orbits shown in Fig. 1 can be figured out by setting $\tau=e^{i\phi}$. Using Eqs. (1) and (2), the condition $|\tau|^2=1$ can lead to $\langle v_x\rangle/\langle v_y\rangle=1$ where $\langle v_x\rangle$ and $\langle v_y\rangle$ are the average speeds along the x and y axes. In other words, the general relation $\tau=e^{i\phi}$ is consistent with the requirement of $\langle v_x\rangle/\langle v_y\rangle=1$ for the classical periodic obits shown in Fig. 1. Substituting Eq. (2) and $\tau=e^{i\phi}$ into Eq. (1) yields

$$\Psi_N(x,y;\phi)=\left(\frac{2}{a}\right)\frac{1}{2^{N/2}}\sum_{K=0}^{N}\binom{N}{K}^{1/2}e^{iK\phi}\times\sin\left[(K+1)\frac{\pi x}{a}\right]\sin\left[(N-K+1)\frac{\pi y}{a}\right]. \tag{3}$$

Figure 2 depicts the ϕ dependence of the wave function $|\Psi_N(x,y;\phi)|^2$ for $N=25$. It can be seen that the behavior of $|\Psi_N(x,y;\phi)|^2$ agrees very well with the classical periodic orbit shown in Fig. 1. Furthermore, the distribution of $|\Psi_N(x,y;\phi)|^2$ illustrates geometrically Bohr's correspondence principle: the velocity of the classical particle is at a minimum at the specular reflection points of the motion, and therefore the distribution has a peak at these points.

The wave function given in Eq. (3) represents a traveling-wave property. The standing-wave representations can be obtained by using $\Psi_N(x,y;\phi)\pm\Psi_N^*(x,y;\phi)$. Including the normalization constant, the standing-wave forms can be expressed as

$$\Psi_N^c(x,y;\phi)=\frac{(2/a)}{\left[\Sigma_{K=0}^{N}\binom{N}{K}\cos^2 K\phi\right]^{1/2}}\sum_{K=0}^{N}\binom{N}{K}^{1/2}\times(\cos K\phi)\sin\left[(K+1)\frac{\pi x}{a}\right]\times\sin\left[(N-K+1)\frac{\pi y}{a}\right] \tag{4}$$

and

$$\Psi_N^s(x,y;\phi)=\frac{(2/a)}{\left[\Sigma_{K=0}^{N}\binom{N}{K}\sin^2 K\phi\right]^{1/2}}\sum_{K=0}^{N}\binom{N}{K}^{1/2}\times(\sin K\phi)\sin\left[(K+1)\frac{\pi x}{a}\right]\times\sin\left[(N-K+1)\frac{\pi y}{a}\right]. \tag{5}$$

The N dependence of the wave pattern $|\Psi_N^c(x,y;\phi)|^2$ is presented in Fig. 3. Here we only show the wave pattern $|\Psi_N^c(x,y;\phi)|^2$ because the wave pattern $|\Psi_N^s(x,y;\phi)|^2$ is generally the same; the value of the parameter ϕ is fixed to be $\pi/2$ for convenient representation. It can be seen that a large quantum number N is not necessary for the localization of the probability density on the classical trajectory. Even so, it should be noted that the wave function in Eqs. (3)–(5) is not a stationary state because the eigenstate components are not degenerate for the Hamiltonian H. Nevertheless, the calculation result shown in Fig. 4 reveals that $\Delta H/\langle H\rangle$ is proportional to $1/N$. In other words, $\Delta H/\langle H\rangle\to 0$ as $N\to\infty$. This result guarantees the coherent state in Eqs. (3)–(5) to be a stationary state in the classical limit.

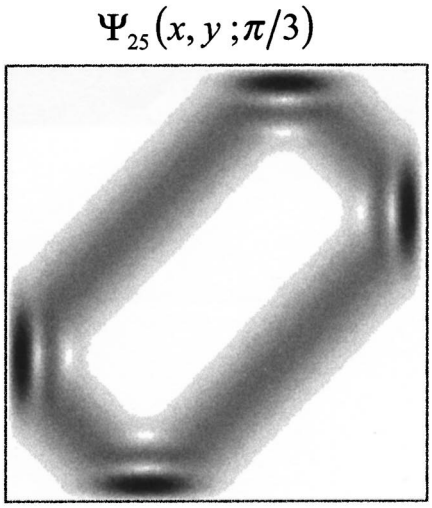

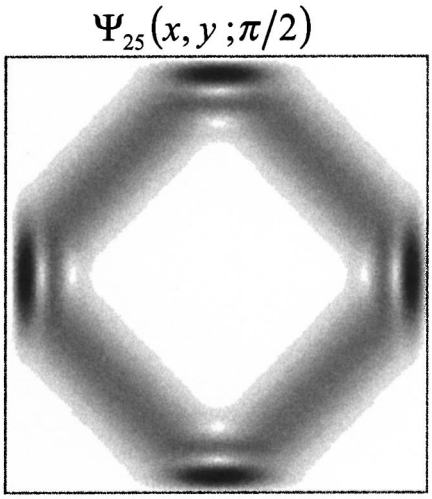

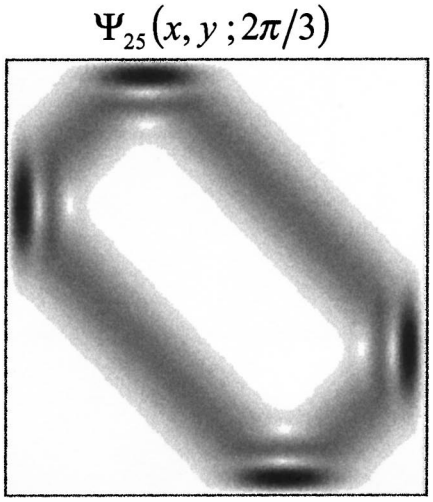

FIG. 2. The ϕ dependence of the wave pattern $|\Psi_N(x,y;\phi)|^2$ from Eq. (3) for $N=25$. The wave patterns correspond to those shown in Fig. 1.

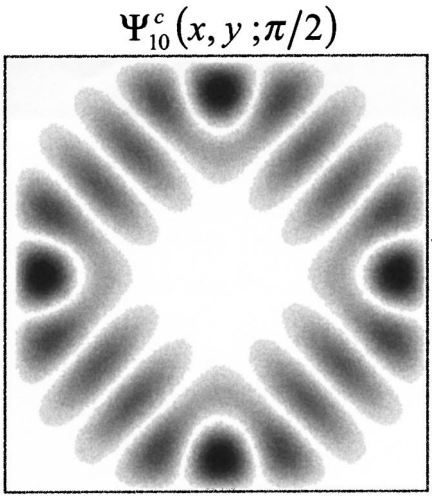

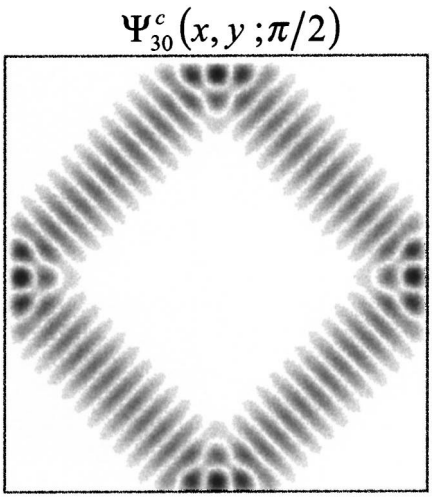

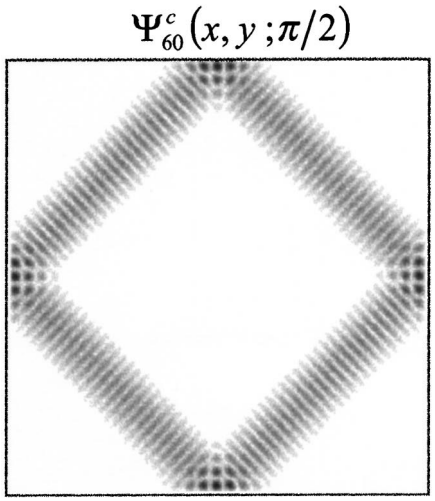

FIG. 3. The N dependence of the wave pattern $|\Psi^c_N(x,y;\phi)|^2$ from Eq. (4) obtained by fixing ϕ to be $\pi/2$ to show the standing-wave property.

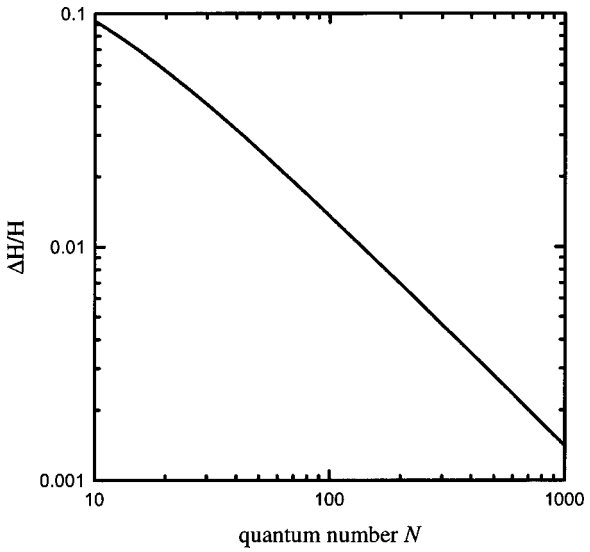

FIG. 4. The calculation result shown for $\Delta H/\langle H\rangle$ versus the quantum number N.

Equations (3)–(5) indicate that the wave function representation consists of $N+1$ Hamiltonian eigenstates. However, the numerical analysis reveals that a superposition of only a few eigenstates is already sufficient to result in the localization on the classical trajectory. To reflect this property, we define the partially coherent states corresponding to Eqs. (3)–(5) as

$$\Psi_{N,M}(x,y;\phi)=\frac{(2/a)}{\left[\Sigma_{K=q}^{N-q}\binom{N}{K}\right]^{1/2}}\sum_{K=q}^{N-q}\binom{N}{K}^{1/2}\exp(iK\phi)\times\sin\left[(K+1)\frac{\pi x}{a}\right]\sin\left[(N-K+1)\frac{\pi y}{a}\right], \tag{6}$$

$$\Psi_{N,M}^{c}(x,y;\phi)=\frac{(2/a)}{\left[\Sigma_{K=q}^{N-q}\binom{N}{K}\cos^2 K\phi\right]^{1/2}}\sum_{K=q}^{N-q}\binom{N}{K}^{1/2}\times(\cos K\phi)\sin\left[(K+1)\frac{\pi x}{a}\right]\times\sin\left[(N-K+1)\frac{\pi y}{a}\right], \tag{7}$$

and

$$\Psi_{N,M}^{s}(x,y;\phi)=\frac{(2/a)}{\left[\Sigma_{K=q}^{N-q}\binom{N}{K}\sin^2 K\phi\right]^{1/2}}\sum_{K=q}^{N-q}\binom{N}{K}^{1/2}\times(\sin K\phi)\sin\left[(K+1)\frac{\pi x}{a}\right]\times\sin\left[(N-K+1)\frac{\pi y}{a}\right], \tag{8}$$

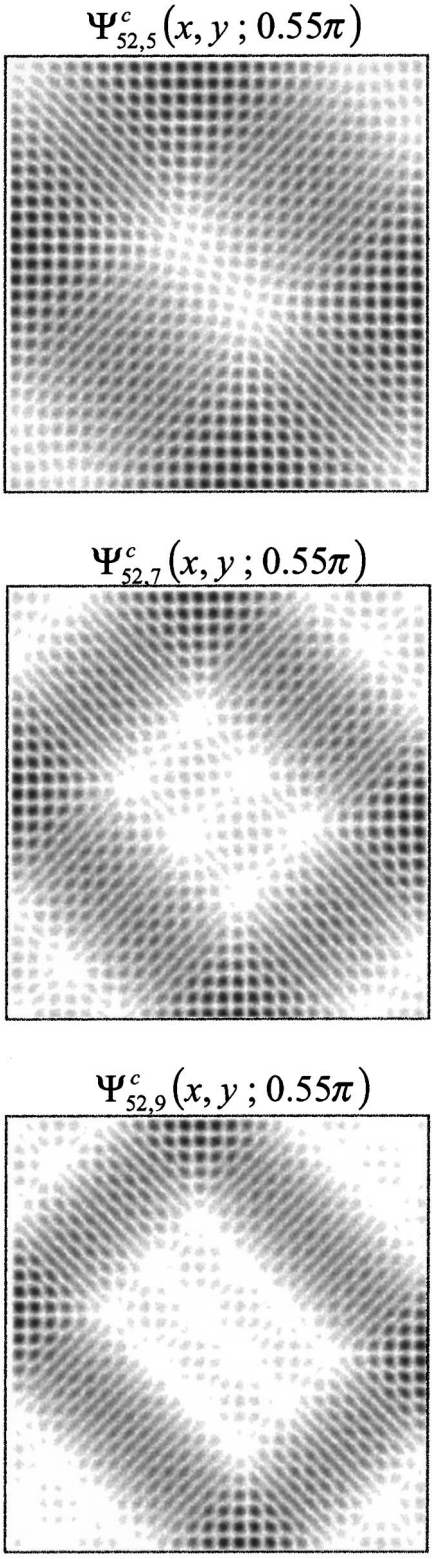

FIG. 5. The M dependence of wave pattern $\Psi_{N,M}^{c}(x,y;\phi)$ from Eq. (7) obtained by fixing ϕ to be 0.55π to show the dependence of wave localization on the number of eigenstates.

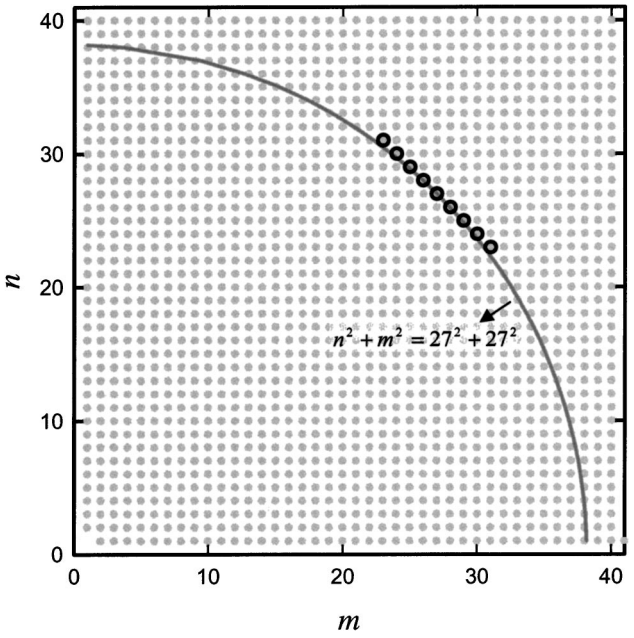

FIG. 6. A diagram illustrating the eigenspectrum of the square billiard. Each gray point represents an eigenvalue; the solid line indicates the curve of the equation $n^2+m^2=27^2+27^2$; the circles are the eigenstates that are selected for the wave patterns shown in Fig. 5.

where the index $M=N-2q+1$ represents the number of eigenstates used in the wave function. All partially coherent states in Eqs. (6)–(8) have similar density localization; we conveniently choose $\Psi^c_{N,M}(x,y;\phi)$ to demonstrate the M dependence of the wave pattern, as shown in Fig. 5. Here we fix ϕ to be 0.55π only for the presentation. It can be seen that only 5–9 eigenstates are adequate to localize the wave pattern on the classical trajectory. The eigenvalue of the energy corresponding to the eigenstate $\psi_{m-1,n-1}(x,y)=(2/a)\sin[m(\pi x/a)]\sin[n(\pi y/a)]$ is given by

$$E=\frac{\hbar^2}{2m}\left(\frac{\pi}{a}\right)^2(m^2+n^2). \tag{9}$$

The degenerate eigenstate depends on the sum of two integer squares (m^2+n^2). Figure 6 shows that the eigenstates of the partially coherent states in Fig. 5 are not exactly degenerate but nearly degenerate. The partially coherent states in Eqs. (6)–(8) may often become the eigenstates in weakly perturbed 2D square billiards [16,17] because they can be composed of only a few nearly degenerate eigenstates. In fact, the wave patterns, like partially coherent states to be localized on classical periodic orbits, have been discussed extensively in ballistic quantum dots [20,21]. In the following section, we demonstrate that the wave patterns of the partially coherent states can be experimentally observed using the transverse pattern formation of a confined microcavity laser.

III. EXPERIMENTAL RESULTS AND DISCUSSION

Recently, vertical-cavity surface emitting semiconductor lasers (VCSEL's) of large transverse section and short cavity length have been used to study the transverse pattern formation [22–25]. VCSEL's inherently emit a single-longitudinal-mode wave because of their extremely short cavity length. The single-longitudinal-mode laser is a useful laboratory to study transverse phenomena without the influence of other degrees of freedom. Hegarty *et al.* [24] reported interesting transverse mode patterns from oxide-confined square-shaped VCSEL's with large aperture. Their experimental results revealed that a wave incident upon the current-guiding oxide boundary would undergo total internal reflection because of large index discontinuities between the oxide layer and the surrounding semiconductor material. In other words, the VCSEL cavity can be considered as a planar waveguide with a dominant wave vector along the vertical direction.

According to the waveguide theory [26], the electromagnetic fields with a predominantly z direction of propagation can be approximated as

$$\vec{E}(x,y,z,t)=\vec{E}(x,y)e^{i(\beta z-\omega t)}, \tag{10}$$

where ω is the angular frequency and β is the propagation constant along the z direction. Using expression (10) in the Maxwell equations for a uniform medium gives the well-known Helmholtz equation [26]

$$[\nabla_t^2+(k^2-\beta^2)]\vec{E}=\vec{0}, \tag{11}$$

where ∇_t^2 is the transverse part of the Laplacian operator, k is the total propagation constant related to the angular frequency by $k=\omega/c$, and c is the wave speed. In fact, lasing modes in a conventional laser are usually characterized by near-paraxial propagation normal to the resonator mirrors, with polarization in the plane of the mirrors [27,28]. Within the framework of the scalar paraxial approximation, the magnitude of the longitudinal field $|E_z|$ is very much smaller than that of the transverse field $|E_t|$ [27]. Therefore, transverse modes in a vertical-cavity laser can be determined by the Helmholtz equation for the transverse field. The solutions to the Helmholtz equation with total internal reflection boundaries ($E_t=0$ at the boundary) are equivalent to the solutions of the 2D Schrödinger equation with hard wall boundaries ($\Psi_N=0$ at the boundary) of the same geometry. Recently, Doya *et al.* [29,30] have introduced the paraxial approximation to establish an analogy between light propagation along a multimode fiber and quantum confined systems. Actually, the guiding character in the oxide-confined VCSEL's is similar to that in optical fibers. Even so, the transverse patterns of VCSEL's under cw operation correspond truly to stationary states of the system.

Due to the analogy between the Schrödinger and Helmholtz equations [18], it is essentially feasible to use the oxide-confined VCSEL cavities like microwave cavities [31,32] to represent quantum mechanical potential wells. In this case, the transverse patterns can reveal the probability density of the corresponding wave functions in the 2D quantum billiards. Here we experimentally study the transverse pattern formation in a square-shaped VCSEL with large aperture to compare with the wave functions in the 2D square billiards.

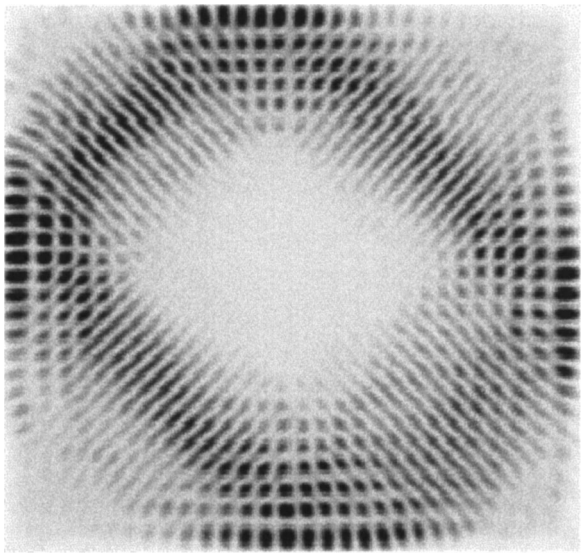

FIG. 7. The experimental result for the near-field pattern of the square-shaped VCSEL device near lasing threshold.

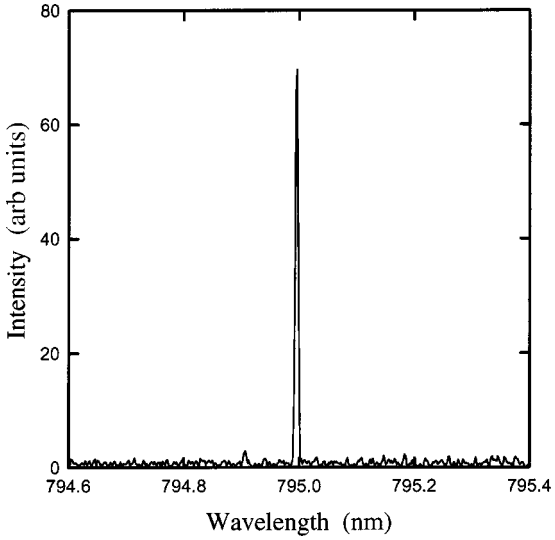

FIG. 8. A plot of the optical spectrum of the transverse pattern shown in Fig. 7.

Square-shaped VCSEL's with large apertures are fabricated by metal organic chemical vapor deposition to emit at a wavelength around $\lambda_z = 795$ nm. The wafers were wet oxidized at 425 °C and the oxidation time is controlled to fabricate a 40 μm oxide aperture in a 110 μm mesa structure. The device structure of these oxide-confined VCSEL's is similar to that described by Ref. [24]. Experimental results show that the transverse patterns of VCSEL's can be evidently divided into two regimes of low-divergence and high-divergence emissions. Hereafter we will concentrate on the high-divergence emission, which appears only at reduced temperature and near-threshold operation. It is expected that the thermal-lensing effect will switch the device into the low-divergence regime because joule heating induces a temperature rise across the device cross section. Typically, high-divergence patterns are very symmetric and those of low divergence are more irregular. Therefore it is easy to differentiate the regimes in which the lasers are being operated.

The near-field patterns are measured with a charge-coupled device camera (Coherent, Beam-Code) and an optical setup similar to that described in Ref. [24]. The transverse mode spectral information of the laser is monitored by an optical spectrum analyzer (Advantest Q8347). The present spectrum analyzer employs a Michelson interferometer with a Fourier spectrum system to reach a resolution of 0.002 nm. The transverse mode spacing can be derived as $\Delta\lambda_t \approx \lambda_z^3/(4a^2) = 0.0785$ nm. Since the resolution of the spectrum analyzer is 0.002 nm, the transverse mode spectral information can be clearly resolved. We cooled the device to a temperature around 0–10 °C. Near lasing threshold the transverse pattern emitted from the present VCSEL device is found to be linearly polarized and highly concentrated along the classical orbit, as shown in Fig. 7. The measurement of the optical spectrum for the laser beam is depicted in Fig. 8. The result reveals that the linearly polarized transverse pattern is a single-frequency oscillation; namely, it is a stationary state. The excellent similarity between the experimental transverse pattern and the wave pattern of the partially coherent state shown in Fig. 6 indicates that the experimental transverse pattern can be described in terms of a few nearly degenerate eigenstates of a perfect square billiard. The optical spectrum information shown in Fig. 8 implies that the nearly degenerate modes are phase synchronized to a common frequency by the mechanism of cooperative frequency locking [33]. Previous laser experiments have proved cooperative frequency locking to be an important process in transverse pattern formation [34–36]. As seen in Fig. 6, a lot of nearly degenerate modes can be selected in the process of cooperative frequency locking. However, the mode selection rule is based on the criterion that the resultant field structure should have the minimum mode volume for the lowest lasing threshold. The criterion of a minimum-volume mode that corresponds to the minimum free energy is equivalent to wave localization along the classical trajectory. This is why the experimental transverse patterns have a connection with the partially coherent states related to classical trajectories. This result confirms that the wave functions related to classical periodic orbits provide a more physical description of a phenomenon than the true eigenstates in mesoscopic systems.

IV. CONCLUSIONS

We have analytically connected the wave function with the classical periodic trajectory in a square billiard using the representation of SU(2) coherent states. We have further modified the analytical form to demonstrate that only a few nearly degenerate eigenfunctions are already adequate to result in the localization of the wave pattern on the classical periodic trajectory. In the experiment, we use the analogy between the Schrödinger and Helmholtz equations to study the features of wave functions from transverse pattern formation in a laterally confined microcavity laser. In a square-shaped microcavity, the experimental transverse pattern agrees very well with the theoretical wave pattern concen-

trated along classical periodic orbits. The experimental result evidences that the wave function obtained as a linear superposition of a few nearly degenerate eigenstates can provide a more physical description of a phenomenon than the true eigenstates in mesoscopic systems.

ACKNOWLEDGMENT

The authors thank the National Science Council for their financial support of this research under Contract No. NSC-91-2112-M-009-030.

[1] J. Wiersig, Phys. Rev. E **64**, 026212 (2001).
[2] J. A. de Sales and J. Florencio, Physica A **290**, 101 (2001).
[3] M. Brack and R. K. Bhaduri, *Semiclassical Physics* (Addison-Wesley, Reading, MA, 1997), Sec. 2.7.
[4] F. von Oppen, Phys. Rev. B **50**, 17 151 (1994).
[5] M. V. Berry, Proc. R. Soc. London, Ser. A **423**, 219 (1989).
[6] E. B. Bogomolny, Physica D **31**, 169 (1988).
[7] O. Agam and S. Fishman, Phys. Rev. Lett. **73**, 806 (1994).
[8] M. C. Gutzwiller, *Chaos in Classical and Quantum Mechanics* (Springer-Verlag, New York, 1990).
[9] S. W. McDonald and A. N. Kaufman, Phys. Rev. Lett. **42**, 1189 (1979).
[10] M. L. Mehta, *Random Matrices*, 2nd ed. (Academic, San Diego, 1991).
[11] J. P. Bird, R. Akis, D. K. Ferry, D. Vasileska, J. Cooper, Y. Aoyagi, and T. Sugano, Phys. Rev. Lett. **82**, 4691 (1999).
[12] Y. H. Kim, M. Barth, H. J. Stöckmann, and J. P. Bird, Phys. Rev. B **65**, 165317 (2002).
[13] I. V. Zozoulenko and K. F. Berggren, Phys. Rev. B **56**, 6931 (1997).
[14] K. Wódkiewicz and J. H. Eberly, J. Opt. Soc. Am. B **2**, 458 (1985).
[15] Vladimir Bužek and T. Quang, J. Opt. Soc. Am. B **6**, 2447 (1989).
[16] R. Narevich, R. E. Prange, and O. Zaitsev, Phys. Rev. E **62**, 2046 (2000).
[17] W. Li, L. E. Reichl, and B. Wu, Phys. Rev. E **65**, 056220 (2002).
[18] J. J. Hupert and G. Ott, Am. J. Phys. **34**, 260 (1966).
[19] J. Pollet, O. Méplan, and C. Gignoux, J. Phys. A **28**, 7282 (1995).
[20] R. Akis, D. K. Ferry, and J. P. Bird, Phys. Rev. Lett. **79**, 123 (1997).
[21] R. Akis, D. K. Ferry, J. P. Bird, and D. Vasileska, Phys. Rev. B **60**, 2680 (1999).
[22] M. Brambilla, L. A. Lugiato, F. Prati, L. Spinell, and W. J. Firth, Phys. Rev. Lett. **79**, 2042 (1997).
[23] C. Degen, I. Fischer, and W. Elsäßer, Opt. Express **5**, 38 (1999).
[24] S. P. Hegarty, G. Huyet, J. G. McInerney, and K. D. Choquette, Phys. Rev. Lett. **82**, 1434 (1999).
[25] T. Ackemann, S. Barland, M. Cara, S. Balle, J. R. Tredicce, R. Jäger, M. Grabherr, M. Miller, and K. J. Ebeling, J. Opt. B: Quantum Semiclassical Opt. **2**, 406 (2000).
[26] J. D. Jackson, *Classical Electrodynamics* (Wiley, New York, 1975), Chap. 8.
[27] A. E. Siegman, *Lasers* (University Science Books, Mill Valley, CA, 1986), Chap. 16.
[28] H. Kogelnik and T. Li, Appl. Opt. **5**, 1150 (1966).
[29] V. Doya, O. Legrand, F. Mortessagne, and C. Miniatura, Phys. Rev. Lett. **88**, 014102 (2002).
[30] V. Doya, O. Legrand, F. Mortessagne, and C. Miniatura, Phys. Rev. E **65**, 056223 (2002).
[31] S. Sridhar, Phys. Rev. Lett. **67**, 785 (1991).
[32] J. Stein and H. J. Stöckmann, Phys. Rev. Lett. **68**, 2867 (1992).
[33] L. A. Lugiato, C. Oldano, and L. M. Narducci, J. Opt. Soc. Am. B **5**, 879 (1988).
[34] J. Scheuler and M. Orenstein, Science **285**, 230 (1999).
[35] Y. F. Chen and Y. P. Lan, Phys. Rev. A **64**, 063807 (2001).
[36] Y. F. Chen and Y. P. Lan, Phys. Rev. A **65**, 013802 (2002).